

MEASUREMENT OF DETECTOR RESPONSE FUNCTIONS FOR FAST NEUTRON SPECTROSCOPY WITH ORGANIC SCINTILLATORS

T. Hutton*, Z. Ndabeni, K. Maibane, E. Jarvie, A. Buffler
Metrological and Applied Sciences University Research Unit,
Department of Physics, University of Cape Town, Cape Town, South Africa

Abstract

Spectrum unfolding decouples spectroscopic measurements of neutron fields from accelerator facilities by making use of a well-characterised detector response matrix. Measurements of detector response matrices, derived from time-of-flight, were made at the fast neutron facility at iThemba LABS, South Africa, with neutrons with energies between 10 - 65 MeV for: a traditional BC-501A organic liquid scintillator detector with photomultiplier tube and analogue pulse processing and acquisition; and a modern system comprised of an EJ-276 plastic scintillator, silicon photomultiplier and digital pulse processing and acquisition. The detector response matrices were validated by unfolding neutron energy spectra from measured light output spectra, and compared to the associated energy spectra derived from time-of-flight. Both detector systems demonstrated good agreement between the energy spectra derived from time-of-flight, which is promising for fast neutron spectroscopy with organic scintillators in environments outside of the laboratory.

CONTEXT

Fast neutron fields with energies up to several GeV are a concern for aviation, manned space missions, workplace exposure and radiation therapy [1-3], and are often poorly understood due to a lack of appropriate measurement devices and reference facilities. In aviation environments the interaction of cosmic rays in the atmosphere and aircraft material produces a shower of secondary radiation with complex composition and energy distribution. At an altitude of 11 km fast neutrons contribute up to 40% of the equivalent dose [4], with peaks in the energy spectrum around 1 MeV and 100 MeV [5], and during unpredictable, short-lived space weather events, the flux of cosmic rays, and secondary neutrons, increases dramatically [6]. Fast neutron interactions with biological or electronic matter cause indirect damage through the production of ionising reaction products, which results in an increased risk to both people and electronic systems [7, 8] and requires continuous monitoring to properly assess, and regulate, the radiation exposure of aircrew. The recent developments of solid (plastic) scintillators capable of pulse shape discrimination (PSD), low-voltage silicon photomultipliers (SiPMs) and digital data acquisition, coupled with spectrum unfolding now offers a viable solution to the development of a compact fast neutron spectrometer, which is suitable for use in a range of applications, including dosimetry in aircraft. We present the

measurement and validation of detector response functions for fast neutrons (10 – 65 MeV) with a traditional liquid scintillator and NIM-electronics based system, and a compact detector system utilising modern acquisition technologies.

MEASUREMENTS

Measurements were made at the iThemba LABS (iTL) fast neutron facility [9, 10], where ns-pulsed fast neutron beams are produced in the energy range of 30 - 200 MeV using proton beams from the $k = 200$ cyclotron. The time spread of a proton bunch is approximately 1 ns, and a beam pulse selector is used to increase the time between bunches up to 360 ns. Neutrons were produced using a beam of 66 MeV protons incident on an 8.0 mm thick ^{nat}Li target. The neutron energy spectrum is comprised of a forward-biased mono-energetic peak from the $^7\text{Li}(p, n)^7\text{Be}$ reaction, which proceeds only by the transition to the ground state and the first excited state of ^7Be , with all higher levels being unstable [11], and a nearly isotropic, lower energy continuum that extends up to the primary peak [12]. Neutron beams are produced at 0° and 16° relative to the incident proton beam using a 2.0 m thick steel collimator (5.0 x 5.0 cm² apertures).

In time-of-flight spectroscopy [13], a ns-pulsed beam of ions are incident on a neutron producing target, and the time of arrival T of those neutrons reaching a detector is measured for a known distance d . The neutron energy E_n can then be determined from:

$$E_n = mc^2 \left[\frac{1}{\sqrt{1 - (d/cT)^2}} - 1 \right] \quad (1)$$

where m is the rest-mass of a neutron, and c is the speed of light.

Measurements were made with a \varnothing 5.1 cm x 10.2 cm BC-501A organic liquid scintillation detector at 0° and at $d = 8.0$ m from the ^{nat}Li target, and data were acquired in coincidence in list-mode for time-of-flight (T), pulse shape (S) and pulse height (L) parameters using a NIM-based acquisition system (Fig. 1). The pulse shape parameter S is determined by the zero-crossover method and is implemented with a FAST ComTec 2160A module [14] on the fast anode output. Neutron only events are separated from gamma ray events as indicated by the dashed line in the L - S histogram in Fig. 2. The pulse height parameter L is calibrated with known gamma ray sources to produce a MeV electron-equivalent (MeV_{ee}) scale. The time-of-flight parameter T was calibrated by inserting several delays of known length

* tanya.hutton@uct.ac.za

between the start and stop of the time-to-amplitude converter (TAC) shown in Fig. 1, and by the time of arrival of the gamma ray flash produced at the target.

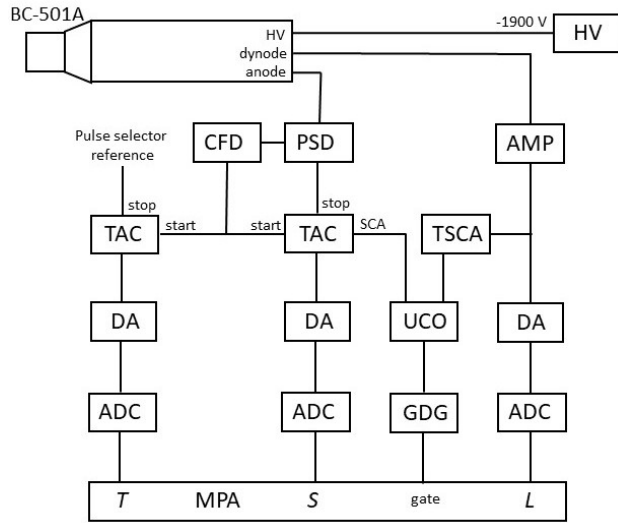


Figure 1: Schematic of NIM-based pulse processing for a BC-501A detector to record time-of-flight (T), pulse shape (S) and pulse height (L) parameters in coincidence with.

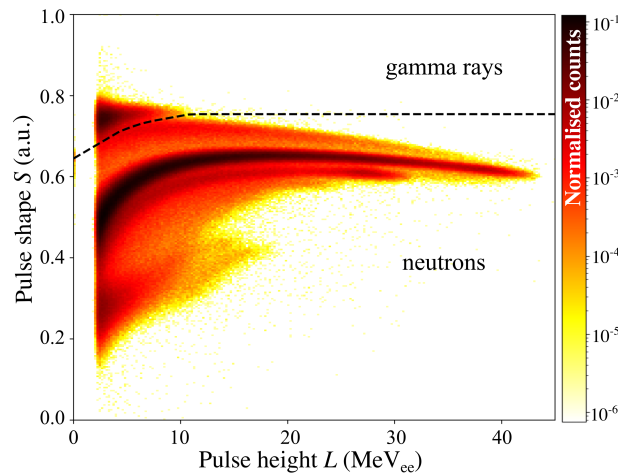


Figure 2: Distribution of events as a function of pulse height parameter L and pulse shape parameter S measured with a BC-501A detector at 8.0 m and 0° for a 66 MeV proton beam on an 8.0 mm ^{nat}Li target.

The compact spectrometer shown is shown in Fig. 3, which comprised of a $6 \times 6 \times 120 \text{ mm}^3$ EJ-276 [15] scintillator optically coupled to a MicroFC-60035 [16] silicon photomultiplier (SiPM). Full waveform data were acquired in list mode using a CAEN DT5730 [17] digitizer and Qt-DAQ [18] software for offline processing. Figure 4 shows the L - S histogram measured for the compact detector at 16° and 8.0 m from the ^{nat}Li target. The light output parameter L was determined from the integral of the SiPM pulse and calibrated with a series of known gamma ray sources,

and the shape parameter S was calculated according to the charge comparison method of pulse shape discrimination (PSD) [19]. Neutron events were separated as indicated by the dashed line. The time-of-flight parameter T was determined from the time difference between the detected event and the reference pulse associated with the proton beam, where both waveforms were acquired in coincidence and a software implemented digital constant fraction discriminator [11] was used to determine the time associated with the reference pulse and radiation induced event.



Figure 3: The compact spectrometer comprised of an EJ-276 scintillator optically coupled to a silicon photomultiplier, with an aluminium and 3D printed casing.

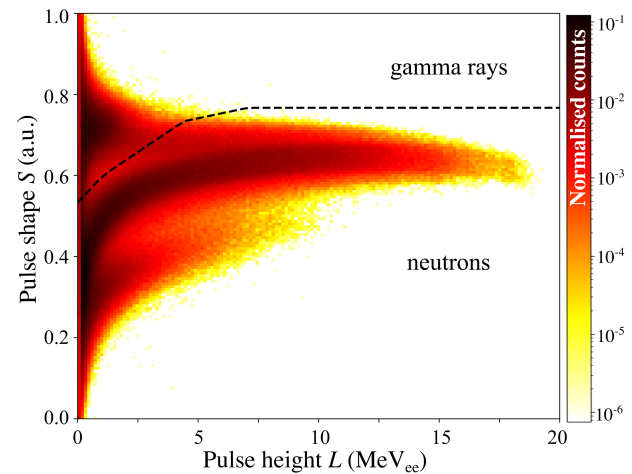


Figure 4: Distribution of events as a function of pulse height parameter L and pulse shape parameter S measured with an EJ-276 detector at 8.0 m and 16° for a 66 MeV proton beam on an 8.0 mm ^{nat}Li target.

RESULTS AND ANALYSIS

Time-of-flight

Figure 5 shows the time-of-flight spectra measured at $d = 8.0 \text{ m}$ for a 66 MeV proton beam irradiating an 8.0 mm ^{nat}Li target. Measurements were made with the BC-501A and EJ-276 detector systems at 0° and 16° respectively. For each detector system the gamma ray contributions were excluded via PSD (Fig. 2, 4), and Eq. (1) was used to derive the neutron energy spectra, which are shown in Fig. 6. The measurement at 0° shows an enhancement at $63.2 \pm 0.3 \text{ MeV}$ associated with the forward-biased $^7\text{Li}(p, n)^7\text{Be}$ reaction

relative to the measurement at 16°, and the lower energy continuum has a similar shape at both measurement angles.

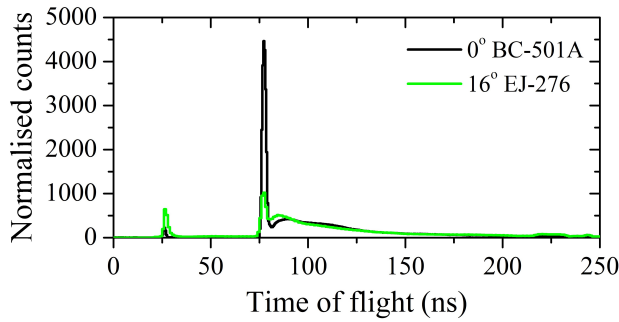


Figure 5: Time-of-flight spectra measured at 8.0 m with a BC-501A detector at 0° and EJ-276 detector at 16° for a 66 MeV proton beam on an 8.0 mm ^{nat}Li target.

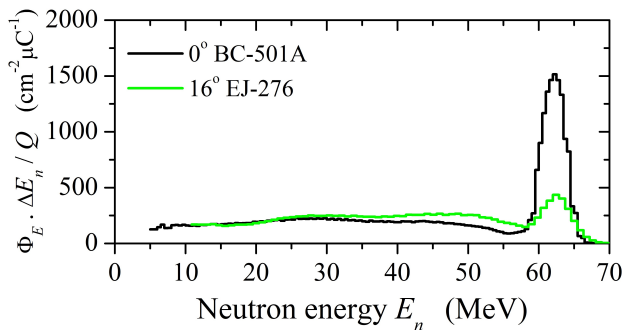


Figure 6: Neutron energy spectra derived by time-of-flight measured at 8.0 m with a BC-501A detector at 0° and EJ-276 detector at 16° for a 66 MeV proton beam on an 8.0 mm ^{nat}Li target.

Spectrum Unfolding

In spectrum unfolding, the neutron energy spectrum is deconvolved from the measured neutron light output spectrum using a known detector response matrix coupled with an unfolding algorithm, and can be used in situations where time-of-flight is unavailable. For organic scintillators, the detector response matrix is comprised of a series of normalised light output spectra for mono-energetic neutrons incident on the detector, which can reliably be simulated for neutron energies below 20 MeV [20]. At higher energies the range of the recoil particles and the increase in available n-C reaction channels results in unreliable response functions derived from calculation [21]. As the quality of the unfolded neutron energy spectrum is entirely dependent on the quality of the detector response functions, these must be measured above 20 MeV.

A detector response matrix was obtained for each detector by selecting energies, derived from time-of-flight, between 10 - 65 MeV in steps of 0.5 MeV (BC-501A) or 3.0 MeV (EJ-276), and calculating the L spectrum associated with that range. As the measured statistics were better for the

BC-501A system due to a larger detection volume, a finer binning structure could be obtained both in L and E . The individual light output spectra were normalised to unity and a selection of these are shown in Fig. 7.

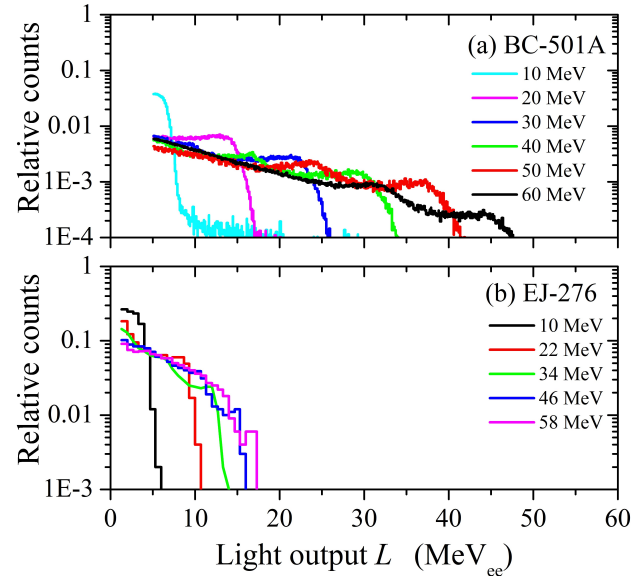


Figure 7: A selection of measured neutron response functions between 10 – 65 MeV for the (a) BC-501A and (b) EJ-276 detector systems.

A superior L resolution is observed in the response functions measured with the BC-501A detector, which is most noticeable in the high- L region associated with the proton recoil edge, and is attributed to the larger light collection area of the detector.

The measured detector response matrices were then used to unfold the neutron light output spectra measured for 66 MeV protons incident on an 8.0 mm ^{nat}Li target at 0° for the BC-501A detector, and 16° for the EJ-276 detector. Figure 8 shows the measured L spectra for the two detector systems alongside the refolded spectra obtained using MAXED [22] with a flat default spectrum and a target χ^2 of 1.0. The solution energy spectra are shown in Fig. 9. For the reference detector system, the energy spectra derived from time-of-flight and unfolding are in good agreement, both in the peak energy (63.0 ± 0.6 MeV) and the overall shape of the continuum. For the compact detector system, the peak energy is well matched within uncertainties (62.5 ± 0.9 MeV), but there are some inconsistencies observed between 30 - 50 MeV, which suggests that the response functions in this region are not sufficiently unique and is attributed to poorer light collection characteristics.

CONCLUSION

Detector response functions were measured at the iThemba LABS fast neutron facility using time-of-flight spectroscopy for neutrons with energies between 10 - 65 MeV for a traditional BC-501A and compact EJ-276 detector systems. Energy spectra were unfolded using MAXED

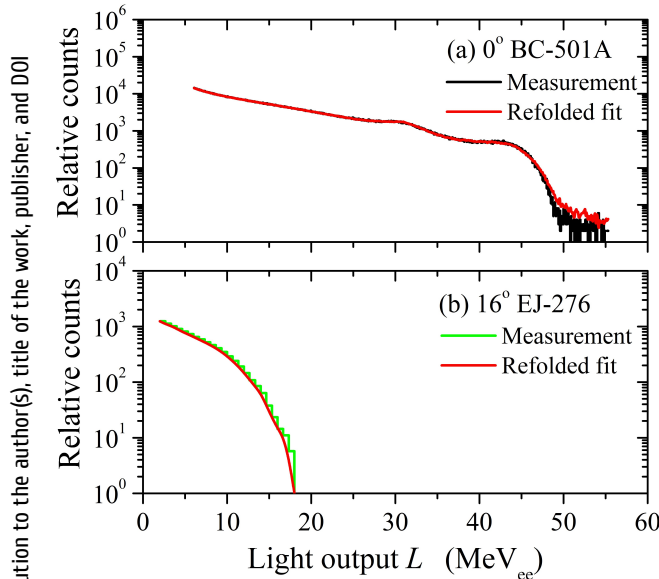


Figure 8: Measured and refolded L spectra for neutrons at 8.0 m with a (a) BC-501A detector at 0° and (b) EJ-276 detector at 16° for a 66 MeV proton beam on an 8.0 mm ^{nat}Li target

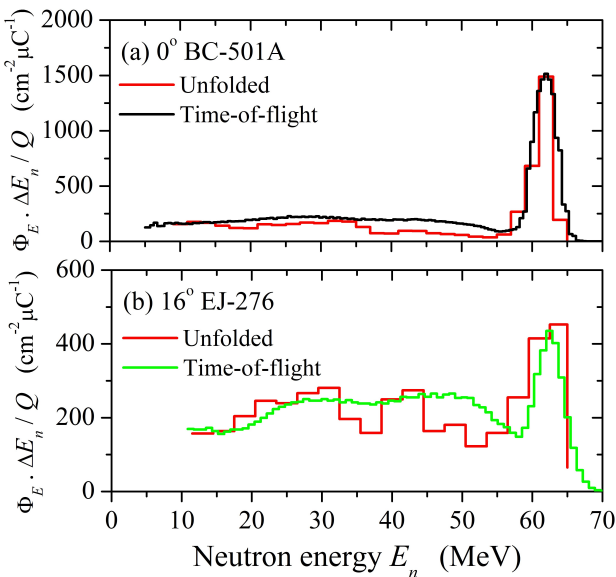


Figure 9: Neutron energy spectra unfolded with MAXED for the BC-501A and EJ-276 detectors and compared the time-of-flight derived energy spectra.

and were comparable to those measured by time-of-flight, which is promising for fast neutron spectroscopy with organic scintillators outside of the traditional laboratory environment. The quality of the energy spectrum unfolded using the compact detector response matrix was limited by low measurement statistics, and a poor L resolution. A significant improvement in L resolution is expected with the addition of a second SiPM to double the light collection area[ref], and further measurements are planned for ener-

gies up to 200 MeV to improve the statistics of the response functions and extend the range of applications. The compact detector system developed as part of this work forms one of the key work packages associated with the South African Space Neutron Initiative (SASNI)¹ and will be used for spectral measurements of cosmic ray induced neutrons at aviation altitudes.

ACKNOWLEDGEMENTS

This work was partially funded by the National Research Foundation (NRF), grant number 138069.

REFERENCES

- [1] P. Grieder, *Cosmic Rays at Earth: Researcher's Reference Manual and Data Book*, Elsevier, 2001.
- [2] J. M. Clem *et al.*, *Rad. Prot. Dos.*, vol. 110, nos. 1-4, p. 423, 2004.
- [3] M. Bagshaw and P. Illig, *Travel Medicine*, 4th Ed., Elsevier, 2019.
- [4] C. J. Guembou Shouop *et al.*, *Eur. Phys. J. Plus*, vol. 135, p. 438, 2020.
- [5] P. Goldhagen *et al.*, *Rad. Prot. Dos.*, vol. 110, p. 387, 2004.
- [6] P. Beck, "Aircraft Crew Radiation Exposure in Aviation Altitudes During Quiet and Solar Storm Periods", in *Space Weather*, Ed. J. Liliensten, Springer, 2007.
- [7] A. J. Sigurdson and E. Ron, *Cancer Invest.*, vol. 22, no. 5, p. 743, 2004.
- [8] B. Todd and S. Uznanski, Proc. CAS-CERN Accelerator School, CERN, Geneva, Switzerland, Rep. CERN-2015-003, p. 245, 2015.
- [9] M. Mosconi *et al.*, *Rad. Meas.*, vol. 45, no. 10, p. 1342, 2010.
- [10] N. B. Ndlovu *et al.*, "Upgrade of the iThemba LABS neutron beam vault to a metrology facility", in *Proc. 22nd Int. Conf. on Cyclotrons and their Applications (Cyclotrons'19)*, Cape Town, South Africa, Sep. 2019, pp. 181-184. doi:10.18429/JACoW-CYCLOTRONS2019-TUP012
- [11] A. C. Comrie *et al.*, *Nuc. Instrum. Meth. A*, vol. 227, p. 43, 2015.
- [12] A. Buffler *et al.*, "Modern Neutron Detection", *Proc. Technical Meeting*, Int. Atomic Energy Agency, Vienna, Austria, IAEA-TECDOC-1935, p. 209, 2020, <https://www.iaea.org/publications/14690/modern-neutron-detection>
- [13] J. Copley and J. Udovic, *J. Res. Natl. Inst. Stand. Technol.*, vol. 98, no. 1, p. 71, 1993.
- [14] FAST ComTec, Model 2160A Pulse Shape Discriminator, <https://www.fastcomtec.com/fileadmin/fwww/datasheet/nim/2160a.pdf>, accessed 21 Dec. 2022.
- [15] Eljen Technology. EJ-276 plastic scintillator, <https://eljentechnology.com/products/plastic-scintillators/ej-276>, accessed 21 Dec. 2022.

¹ SASNI is comprised of members from the Department of Physics, University of Cape Town, South African National Space Agency (SANS) and iThemba LABS fast neutron and radiation biophysics divisions.

- [16] SensL, C-series silicon photomultiplier, <https://www.onsemi.com/>, accessed 21 Dec. 2022.
- [17] CAEN, DT5730 digitizer, <https://www.caen.it/products/dt5730/>, accessed 21 Dec. 2022.
- [18] A. Comrie, QtDAQ, <https://github.com/veggiesaurus/qtdaq>, accessed 21 Dec. 2022.
- [19] C. Sole *et al.*, *IEEE Trans. Nucl. Sci.*, vol. 69, p. 1780, 2022.
- [20] NRESP-3, Organic Scintillation Detector Response to Monoenergetic Fast Neutron, 26. Oct. 1985, available online: <http://www.nea.fr/abs/html/nea-0700.html>
- [21] A. Buffler *et al.*, *IEEE Trans. Nucl. Sci.*, vol. 62, p. 1422, 2015.
- [22] M. Reginatto, *Nucl. Instrum. Meth. A*, vol. 476, p. 242, 2002.

Content from this work may be used under the terms of the CC-BY-4.0 licence (© 2022). Any distribution of this work must maintain attribution to the author(s), title of the work, publisher, and DOI

